Combustion synthesis: Towards novel nanomaterials

Andrzej Huczko[1,*], Agnieszka Dąbrowska[1], Michał Bystrzejewski[1], Łukasz Dobrzycki[1], Maciej Fronczak[2], Anar Mukhametzhanova[3], Santosh Tiwari[4], Manoj Pandey[5], Rabisharan Bogati[5], Bhim Kafle[5], Deepak Prasad Subedi[5]

Department of Chemistry, Warsaw University, Warsaw, Poland[1]
Department of Molecular Engineering, Faculty of Process and Environmental Engineering, Lodz University of Technology, Lodz[2]
RSE 'National Center on Complex Processing of Mineral Raw Materials of the Republic of Kazakhstan', Almaty, Kazakhstan[3]
Key Laboratory of New Processing Technology for Nonferrous Metals and Materials, School of Resources, Environment and Materials, Guangxi University, Nanning, China[4]
Department of Physics, School of Science, Kathmandu University, Dhulikhel, Kavre, Nepal[5]
ahuczko@chem.uw.edu.pl

Abstract: *The combustion synthesis (CS) is an autogenous and strongly exothermic chemical reaction in a powdered mixture of a strong reducer and oxidizer. Such processes, due to short duration and fast quench, can be a source of novel nanomaterials. Here we present (i) the CS synthesis of SiC nanowires (SiCNWs) and (ii) the magnesiothermic reduction of the asbestos waste. The resulting raw and purified products were analyzed with different chemical and physicochemical techniques (XRD, SEM, TGA and Raman spectroscopy) to verify its composition and morphology.*

Keywords*: COMBUSTION SYNTHESIS, MAGNESIOTHERMIC REDUCTION, SiC NANOWIRES, GRAPHENE, NANOSTRUCTURES, WASTE*

1. Introduction

The bottom-up approach of the synthesis of nanomaterials involves the generation of building blocks (ions, atoms, radicals, molecules) via the thermal or plasma activation of starting reactants. Here we propose the combustion synthesis (CS) which is an autogenous and strongly exothermic redox reaction between oxidizer and reducing agents and has been well known and explored for many years now [1]. For example, the thermite reaction has been widely used for connecting rails, in military applications and fireworks while CS has been routinely utilized in the generation of emergency oxygen on board the aircraft. Combustion synthesis has been also successfully used to produce different nanomaterials [2]. The CS is here an adaptation of a simple and easier synthesis option bestowed with time and energy saving prospect. Huczko et al. [3] produced efficiently silicon carbide nanowires (SiCNWs) in the reaction between elemental silicon and halogenated carbon compounds. The CS approach, due to a short reaction duration and fast quench, may be the source of novel nanocarbons, after removal (acid leaching) of side oxides. We tested the magnesiothermic processing of different mixtures including both model carbon-containing compounds and carbon-related commodities [4] to obtain graphene-related nanocarbons. A metallothermic reduction processes have been also patented [5], i.e. a porous silicon-based material comprising porous crystalline elemental silicon formed by reducing silica can be used to construct negative electrode used in lithium ion batteries [6].

Among various 2D nanomaterials, graphene has received extensive research attention in the last 2-3 decades due to its fascinating properties. The multidisciplinary characteristics of graphene provides a platform for a wide range of applications from health to aerospace. As an example, in September 2019 the first in the world photovoltaic power station (power 1.8 MW) was inaugurated in Feliksów (Poland) in which the photovoltaic silicon-based modules were graphene-modified. Tiwari et al. [7] presented recently the review article providing an outline of graphene in terms of fundamental properties, cutting-edge research and applications.

One should also mention here the solution combustion synthesis (SCS) which ensures uniform distribution and atomic level mixing of reactants in liquids, and yields powders with reduced particle size. As an example, Manjunath et al. [8] successfully synthesized zinc oxide nanoparticles using pigeon pea as a fuel. The as-prepared ZnO showed good photocatalytic and antibacterial activities. Recently, the antimicrobial copper-based precipitates were formed during the SCS using L-ascorbing acid as reducing agent but long (24 hours) reaction duration was a clear disadvantage of that approach [9]. Huczko et al. [10] also applied the SCS approach to produce and characterize YAG:Ce^{3+} garnet nanopowders.

We present here the results of two series of combustion runs. The silicon reduction of fluorinated graphite was aimed not only at the production of SiCNWs but it was also expected that the defluorination of CF_x can lead towards the formation of graphene-like carbon nanostructures. The magnesiothermic reduction of asbestos waste can produce fine silica with some specific surface properties this due to the high temperature and fast quench of the combustion products. The resulting raw and purified products were analyzed with XRD, SEM, EDS, TGA and Raman spectroscopy to verify its composition and morphology.

2. Experimental

Table 1 presents the operational parameters of all runs. The starting stoichiometric components were hand-mixed at ambient temperature prior to introduction into the quartz crucible in reactor before performing the combustion synthesis. The combustion was initiated thermally by ohmic heating of a carbon tape immersed in the reactants following the experimental protocol described elsewhere [11]. The reactor was provided with the observation port to record the light emitted from the combustion zone. The starting pressure in the reactor was either 0.1 or 1.0 MPa. The combustion was terminated within ca 1 second and, after cooling period, the solid raw products were collected for the mass balance and the following analyses. The work-up of product mixtures was carried out by wet chemistry to remove non-converted starting reactants and unwanted side-products.

Table 1*. Operational parameters of combustion syntheses*

Run No.	Starting reactants	Mass of starting reactants, g	Combustion atmosphere	Starting pressure, MPa	Peak pressure, MPa	Mass of raw products, g
I-1	Si + CF_x	4.71	Air	0.1	2.8	3.26
I-2	Si + CF_x	6.63	Air	1.0	7.0	4.53
II-1	Mg + asbestos waste	6.70	Argon	0.1	0.4	6.34
II-2	Mg + asbestos waste	5.48	Argon	1.0	1.4	5.28
II-3	Mg + asbestos waste	5.35	Argon	0.1	1.2	5.32
II-4	Mg + asbestos waste	5.46	Argon	1.0	1.8	5.42

3. Results and Discussion

The exothermal combustion is accompanied by the strong emission of heat and light. The latter one can be a useful source of information about the nature of the reaction and its time. Thus, the Light Signal Diagnostics (LSD) protocol was developed, which enabled the on-line measurement of the reaction duration and characteristics, especially the detailed monitoring of the propagation of the combustion wave and its front. Fig. 1 presents few examples of such results for the selected combustions which confirm the short reaction duration (within ca 1 second) and its susceptibility to even the minor changes in initial operational parameters (such as the pressure and type of gaseous atmosphere). One may also follow the complex time signal trajectory with its oscillations and local combustion wave maxima. They correspond to the kinetics of the process. The light characteristics is reproducible within the same operational conditions. Thus, it can be treated as a reactions fingerprint.

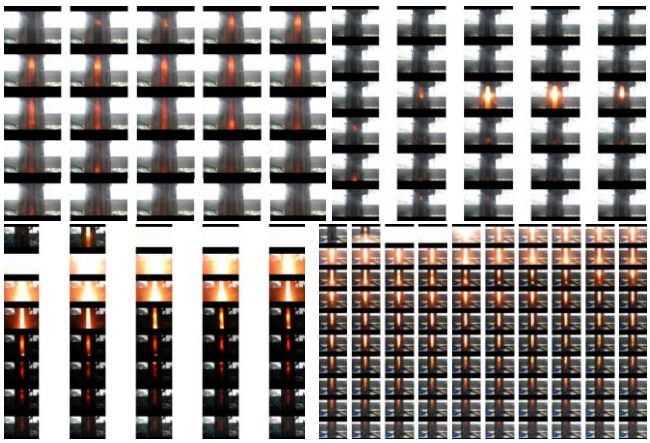

Fig. 1. *The in situ mapping of combustion synthesis for different run; A: run II-4; B: run II-3; C: run I–2; D: run II-1*

As one can see, the combustion in the Si/CF_x is much more vigorous regarding the emission of a light and heat. Different mixtures of reactants may lead to the designed nanomaterials (Fig. 2). The versatility is a crucial advantage of the combustion synthesis. On the other hand, LSD enables its precise diagnostics and facilitates the optimization.

The morphology of raw products is quite different comparing to the starting mixture (Fig. 2). The raw product from combustions in the Si/CF_x systems is amazingly voluminous this due to the high amount of 1D SiC nanostructures.

a) b)

Fig. 2. *Reactants before combustion (left) and raw reaction products (right) from runs; a: run II-4; b: run I-2*

3.1. Synthesis of silicon carbide nanowires (SiCNWs)

The silicon reduction of the fluorinated graphite CF_x (x = 0.89) in air atmosphere follows the general equation

$$Si + CF_x = SiC + C + Si + SiO_2 + \uparrow SiF_4 + \uparrow C_xF_y$$

We showed earlier [12] that the reaction of silicon with halogenated carbons (like TEFLON®) proceeds more efficiently under the presence of oxygen this due to vigorous gas phase mass transport of silicon via gaseous SiO molecules. It was expected that the application of the fluorinated graphite as an oxidizer could enable not only the growth of SiCNWs but also the formation of layered graphene-like carbon nanostructures resulting from the silicon extraction of fluorine from layered graphite matrix. To isolate the SiCNWs, the un-reacted Si and silica were leached with boiled 30% KOH why the residual carbon was removed via air oxidation at 600 ^oC in the following step. The combustion was accompanied by a strong pressure increase (Table 1) this due to the high temperature and formation of gaseous side products ($SiF_4 + C_xF_y$). The latter one is confirmed by a substantial mass decrease of solid reactants (Table 1). The content of un-reacted Si in a raw product (from wet chemistry analyses) for runs I-1 and I-2 was equal to 5.4 and 3.6 wt%, respectively. Thus, the total conversion of starting silicon was very high, 93.0 % and 95.6 % for runs I-1 and I-2, respectively.

Fig. 3 presents the SEM images of the starting mixture (runs I-1 and I-2) composed of several micron-sized Si crystallites (Fig. 3A) and layered CF_x (Fig. 3B).

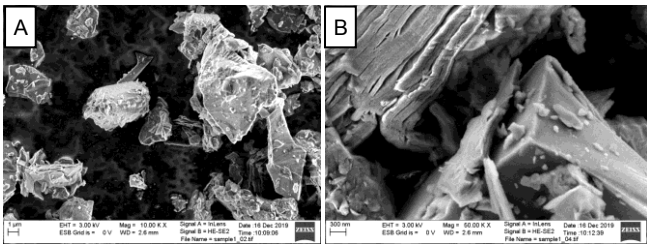

Fig. 3. *SEM images of starting mixture (runs I-1 and I-2*

The morphology of the raw product (Fig. 4) does not depend on the starting pressure. The raw product is a non-homogeneous mixture of different nanosized species including SiCNWs, nanoballs (200-400 nm) of SiO_2, spherical (well below 100 nm) soot particles and microcrystallites of SiC.

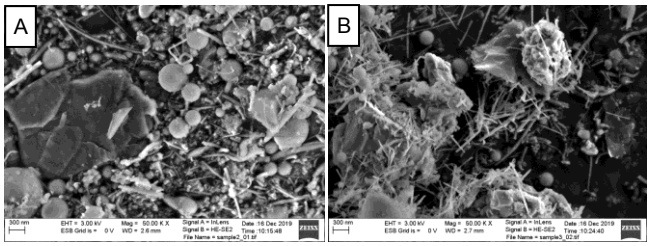

Fig. 4. *SEM images of raw product*

The purified product (Fig. 5) is composed essentially of SiC nanowires (well below 100 nm) with some SiC cubic microcrystallites.

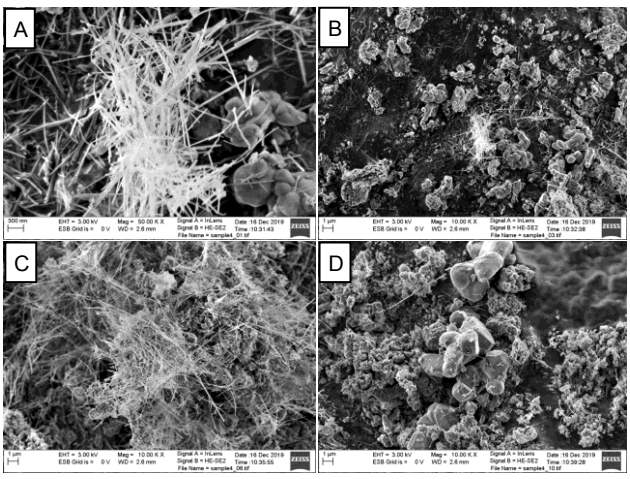

Fig. 5. *SEM images of purified product*

To confirm the purity of the product the EDS analysis was carried out (Fig. 6) which confirmed the stoichiometry of the formed SiC. The results (Table 2) confirm the content of SiC in a purified product above 90 at.%.

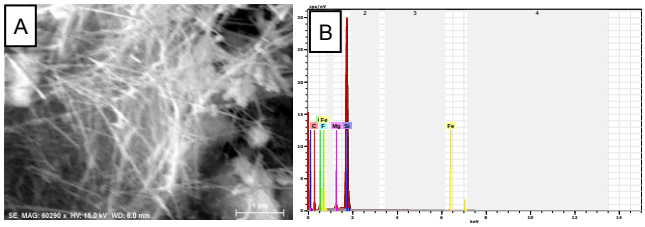

Fig. 6. *EDS analysis of purified product*

Table 3. *EDS analysis of the purified product*

Element [wt.%]	Series	unn. C [wt.%]	norm. C [at.%]	Atom. C [wt.%]	Error (1 Sigma)
Carbon	K-series	28.25	30.01	48.14	4.46
Oxygen	K-series	7.23	7.68	9.25	1.23
Silicon	K-series	56.47	59.99	41.15	2.37
Fluorine	K-series	0.16	0.17	0.17	0.10
Magnesium	K-series	1.16	1.24	0.98	0.09
Iron	K-series	0.85	0.90	0.31	0.08
Total:		94.12	100.00	100.00	

TGA analysis (Fig. 7) confirmed that conclusion. The purified SiCNWs contain less that 5 wt% of carbon which removal from the final product occurs between 500 and 600 ^{o}C.

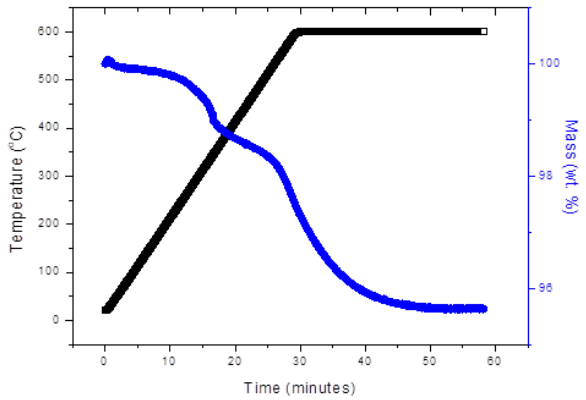

Fig. 7. *TGA analysis of purified SiCNWs product*

Fig. 8 presents XRD spectra of the reactants. The starting mixture (Fig. 8a) is composed of crystalline Si elemental (with some residual Ge presence)) while the CF_x phase seems to be amorphous. The raw product (run I-2, Fig. 8b) contains mostly SiC with some un-reacted silicon while the carbon is evidently in an amorphous form. The purified product (Fig. 8c) is dominated by SiC reflexes.

The results showed that pure SiC nanowires can be efficiently produced via the silicon reduction of the fluorinated graphite. The observations of the product did not reveal, however, the presence of layered carbon nanostructures. Thus, it seems that the extremely strong thermal effect of combustion totally atomizes the carbon (forming the hexagonal network in starting CF_x) which later condenses as amorphous soot.

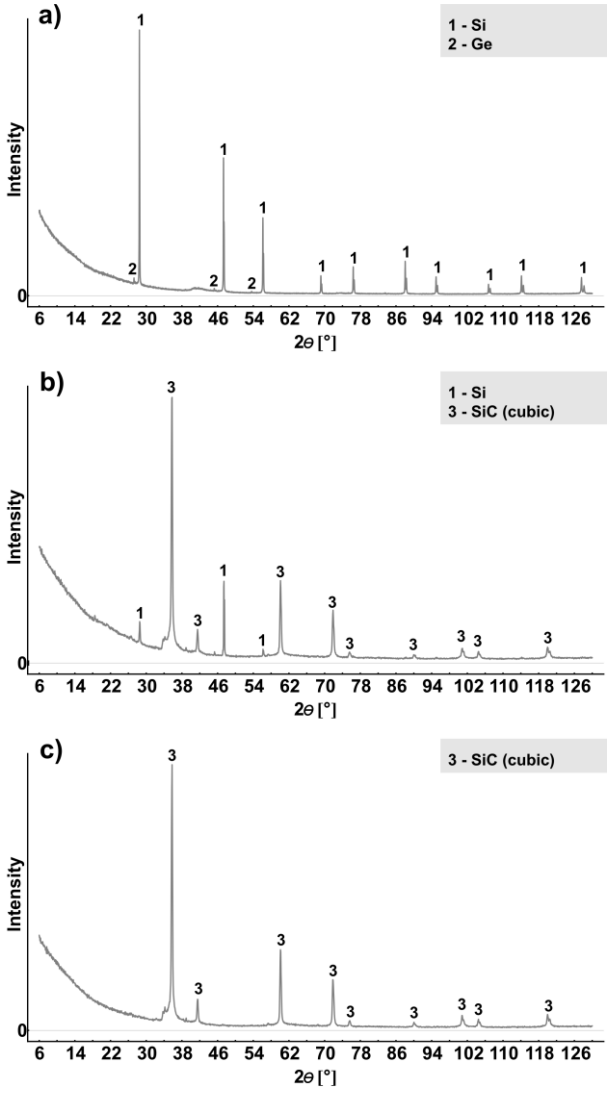

Fig. 8. *XRD spectra of selected samples; run I-2: a – starting mixture; b – raw product, c - purified product*

3.2. Magnesiothermic reduction of asbestos waste

The magnesiothermic processing of asbestos waste [13] with Mg as a reducing agent follows here the general scheme

$$Mg + MgO.SiO_2.H_2O = MgO + Mg + Si + SiO_2 + H_2O$$

Ma et al. [14] earlier produced porous silicon by magnesiothermic reduction of serpentine mineral. It was expected here that the final product, after chemical purification (acid leaching), would contain mostly fine silica (along with Si elemental) with some specific surface properties. As a matter of fact, silica-based amine-grafted sorbents exercised high amine efficiency for CO_2 capture, leading to a record-high CO_2 capacity of ~12 mmol g^{-1} under simulated flue gas conditions [15].

Fig. 9 presents the micrograph of starting asbestos waste which reveals its particle size well below 5 μm and heterogeneous morphology.

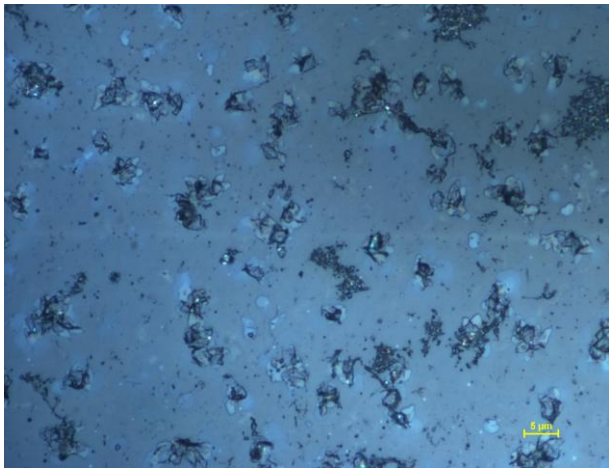

Fig. 9. *Micrograph of asbestos waste*

The combustions were carried out with a two-fold excess of Mg (runs II-1 and II-2) and with a stoichiometric amount of a reducer (runs II-3 and II-4) – Table 1. The mass of the collected raw product did not differ substantially from the starting mass and the pressure increase was quite moderate this all showing that we dealt entirely with the solid-phase reaction. Fig. 10 presents the SEM images of the starting reactants (runs II-3 and II-4), composed of heterogeneous mixture of Mg particles and waste microcrystallites with some residual asbestos fibers.

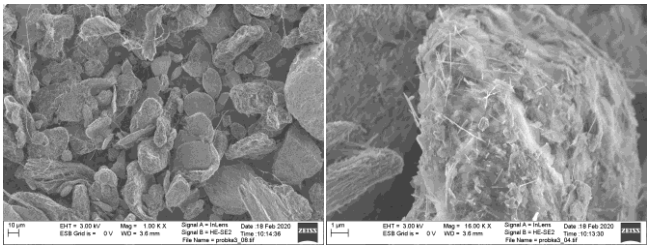

Fig. 10. *SEM images of starting mixture (runs II-3 and II-4)*

The raw product (Fig. 11) has a quite different morphology. There are only very few of asbestos fibers and the material is dominated by cubic nanocrystallites of MgO.

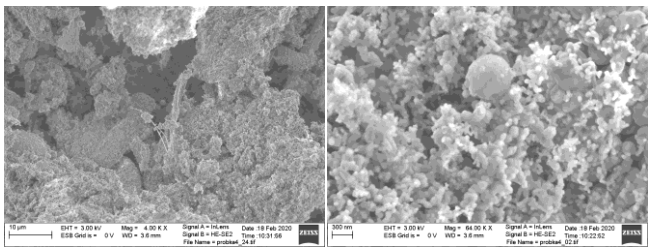

Fig. 11. *SEM images of raw product (runs II-3 and II-4)*

The purified product (Fig. 12) has a heterogeneous morphology; MgO nanocrystallites are essentially gone while some interesting platelet-like porous nanostructures are easily spotted.

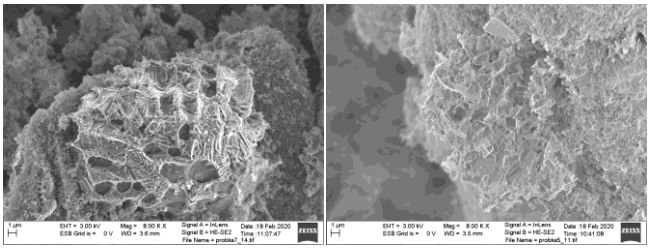

Fig. 12. *SEM images of purified product (run II-3 and II-4)*

To identify its identity the EDS analysis was carried out (Fig. 13).

Table 3. *EDS analysis of the purified product*

Spectrum: Acquisition

Element	Series	unn. C norm. [wt.%]	C Atom. [at.%]	C Error (1 Sigma) [wt.%]
Oxygen	K-series	16.59	17.84	27.83	2.43
Silicon	K-series	74.18	79.74	70.89	3.11
Iron	K-series	1.87	2.01	0.90	0.13
Aluminium	K-series	0.38	0.41	0.38	0.05
Total:		93.03	100.00	100.00	

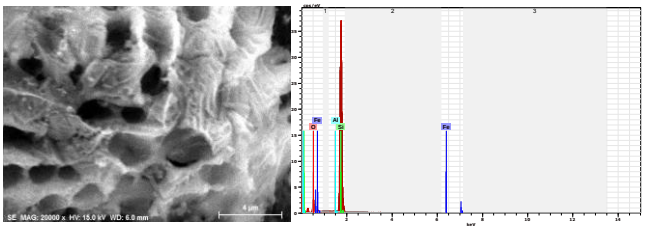

Fig. 13*. EDS analysis of purified product (run II-4)*

The porous material (in a purified product) is mostly composed of the elemental Si with some residual silica – Table 3.

The XRD spectra of reactants are shown in Fig. 14. The starting mixture (run II-4, Fig. 14a) is dominated by Mg elemental with the waste mineral phase (here denoted as a serpentine). The raw product (run II-4, Fig. 14b) contains mostly MgO with some un-reacted magnesium and serpentine, along with other side products. Surprisingly, the purified product (Fig. 14c) is dominated by the elemental silicon (instead of the expected silica) with some iron silicide and silicon carbide (formed from a residual carbon). That result proves that the sought reaction proceeded much deeply and resulted in a magnesiothermic reduction of silica.

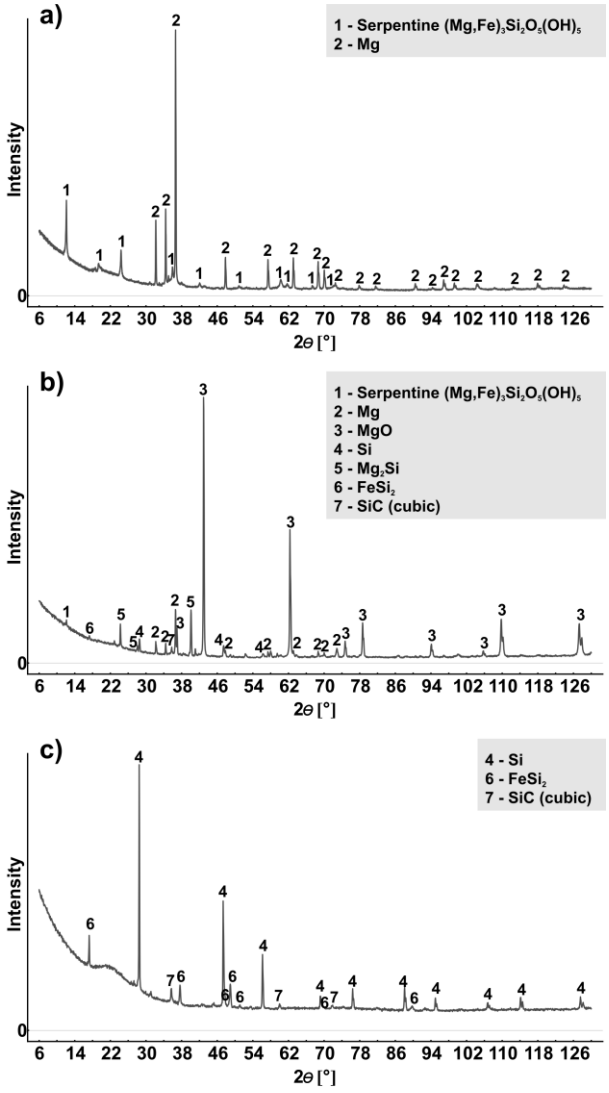

Fig. 14. *XRD spectra of selected samples (run II-4): a – starting mixture; b – raw product, c - purified product*

The adsorption performance of both raw and purified products was analyzed in the process of 4-chlorophenol removal from aqueous solution. The adsorption of raw product (runs II-3 and II-4) was negligible due to the basicity of the surface. However, the surface of the purified products (after leaching with HCl) does not exhibit basic properties. In these cases the adsorption of 4-chlorophenol was detectable and measurable. However, the highest obtained values of the adsorption capacity were not high, namely 12 mg/g and 18 mg/g for run II-3 and II-4, respectively. The obtained adsorption isotherms (Fig. 15) are typical for S1 isotherms in Giles' classification [16] or for the III type in the IUPAC classification [17]. Both correspond to the weak attraction between solute molecules and the surface of the adsorbent.

4. Conclusions

Combustion synthesis was used to produce SiC nanowires and to reduce the asbestos waste. The silicon defluorination of fluorinated graphite yields 95% pure SiCNWs. However, the residual carbon did not form 2D nanostructures, as expected, but condensed as a soot. The asbestos waste, containing mostly silicon-related compounds, was deeply reduced with Mg elemental, but contrary to expectations, the purified product contained almost 50% of elemental Si along with some residual fine silica.

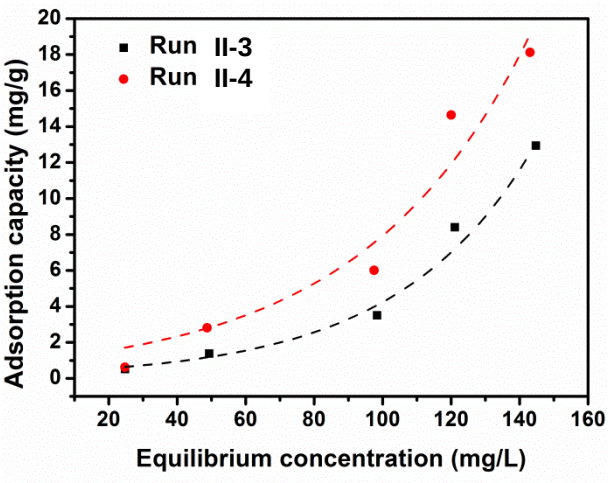

Fig. 15. *Adsorption isotherms for purified products of magnesiothermic reduction of asbestos waste*

5. References

1. J. J. Moore, H.J. Feng, Progr. Mat. Sci., **39**, 275 (1995)
2. A. Huczko, M. Szala, A. Dąbrowska, *Synteza Spaleniowa Materiałów Nanostrukturalnych* (Warsaw University Publishing House, in Polish, 2011)
3. A. Huczko, H. Lange, G. Chojecki, S. Cudziło, Y.Q. Zhu, H.W. Kroto, D.R.M. Walton, J. Phys. Chem. B, **10**, 2519 (2003)
4. A. Dąbrowska, A. Huczko, Phys. Status Solidi B, 255, 1800194 (2018)
5. Patent DE102015221226A1 (2015)
6. Patent WO 147958 A2 (2013)
7. S.K. Tiwari, S. Sahoo, N. Wang, A. Huczko, J. of Sci.: Adv. Mat. Dev., in press (2020)
8. K. Manjunath, T.N. Ravishankar, D. Kumar, K.P. Priyanka, T. Varghese, H.R. Naika, H. Nagabhushana, S.C. Sharma, J. Dupont, T. Ramakrishnappa, C. Nagarju, Mat. Res. Bull., **57**, 325 (2014)
9. 8. A.R. Ramos, A.K.G. Tapia, C.M.N. Pinol, N.B. Lantican, M.I. del Mundo, R.D. Manalo, M.U. Herrera, J. of Sci.: Adv. Mat. Dev., **4**, 66 (2019)
10. A. Huczko, M. Kurcz, P. Baranowski, M. Bystrzejewski, A. Bhattarai, S. Dyjak, R. Bhatta, B. Pokhrel, B.P. Kafle, Phys. Status Solidi B, **250**, 2702 (2013)
11. A. Huczko, A. Dąbrowska, M. Fronczak, M. Bystrzejewski, D.P. Subedi, B.P. Kafle, R. Bhatta, P. Subedi, A. Poudel, Int. J. Self-Prop. High-Temp. Synth., **27**, 72 (2018)
12. M. Soszyński, O. Łabędź, A. Huczko, J. Crystal Growth, **401**, 445 (2014)
13. A. Shayakhmetova, A.A. Mukhametzhanova, I.B. Samatov, D.N., Machines, Technologies, Materials, **13**, 90 (2019)
14. B. Ma, Z. Huang, M. Fang, Y. Liu, S. Chen, Key Eng. Mat., **544**, 29 (2013)
15. G. Qi, L. Fu, E.P. Giannelis, Nature Comm., **5**, 5796 (2014)
16. C.H. Giles, T.H. McEwan, S.N. Nakhwa, D. Smith, J. Chem. Soc., **786**, 3973 (1960)
17. K.S.W. Sing, Pure Appl. Chem., **54**, 2201 (1982)